Progress In Electromagnetics Research, PIER 93, 57–70, 2009

A BREAST IMAGING MODEL USING MICROWAVES AND A TIME DOMAIN THREE DIMENSIONAL RECONSTRUCTION METHOD

H. Zhou †

State Key Laboratory of Petroleum Resources and Prospecting
China University of Petroleum
Changping, Beijing 102249, China

T. Takenaka

Departmen of Electrical and Electronic Engineering
Nagasaki University
Nagasaki, Japan

J. E. Johnson

Miramar Labs, Inc.
Menlo Park, California, USA

T. Tanaka

Department of Electrical and Electronic Engineering
Nagasaki University
Nagasaki, Japan

Abstract—An iterative reconstruction algorithm for three-dimensional (3-D) microwave tomography by using time-domain microwave data is applied to detect breast tumor. A numeric breast model with randomly distributed glandular tissues (random size and permittivity) with a tumor is designed for the calculation of synthetic microwave data. An "air phantom" consisting of a section of polyvinyl chloride (PVC) pipe filled with styrofoam and a thin glass cylinder is constructed for collecting microwave data in laboratory. The "breast" and "air phantom" are reconstructed. Reconstruction results show that the "tumor" in the

Corresponding author: H. Zhou (huizhou@cup.edu.cn).
† Also with Key Laboratory of Geophysical Prospecting, China National Petroleum Corporation, Beijing 102249, China.

breast is clearly reconstructed, and the glass cylinder is successfully reconstructed too.

1. INTRODUCTION

Many women are suffering from breast cancer. Early detection is very helpful for curing it. Several groups are conducting breast cancer detection research [1–6] by using microwave that is safer than X-ray mammography [7]. Among the researched detection techniques some are qualitative methods, and some are quantitative methods.

Recent advances in breast imaging include frequency domain inverse-scattering approaches, such as those by Meany et al., which have demonstrated successful numerical and phantom results [5, 8] and very promising preliminary clinical studies [9, 10]. Additionally, Synthetic Aperture Radar (SAR) based techniques such as Tissue Sensing Adaptive Radar (TSAR) [4, 11] and Microwave Imaging via Space Time Beamforming (MIST) [12, 13] are proposed. They have shown the ability for detecting tumors both in numerical studies and realistic phantom experiments. In fact, the studies carried out by Hagness et al. [14, 15] initiated the recent high level of research activity in microwave imaging of breast cancer. Recently, Lazebnik et al. and Zastrow et al. performed important studies of the ultrawideband microwave dielectric properties of normal, benign and malignant breast tissues [16, 17], and Zastrow et al. created an anatomically realistic numerical breast model [18]. Results showed that the contrast between glandular and malignant breast tissue is not so high as expected. This implies that the breast cancer detection is more difficult and challenging than it was thought.

There are two kinds of quantitative reconstruction methods conducted in the frequency and time domains respectively. In the last two decades various inversion methods in the frequency and time domains suitable for large-size and high-contrast objects have been developed. Several approaches in the frequency domain are developed to reconstruct 3-D objects [19–23]. In the time-domain we have developed a reconstruction technique which is named forward-backward time-stepping (FBTS) method [3]. In this reconstruction method, the gradients of a cost function to unknown parameters are expressed explicitly by introducing an adjoint field, which is calculated by using the finite-difference time-domain (FDTD) method [24, 25]. The cost function is minimized iteratively by using the conjugate gradient method.

This paper considers microwave imaging of relative permittivity

profile in a breast in order to discriminate malignant tissue. In this preliminary work, a non-dispersive and lossless breast model with a high dielectric contrast is used. The FBTS method is applied to the reconstruction of the 3-D breast model. The effectiveness of the imaging technique based on the FBTS inverse scattering analysis is assessed via experimental measurement as well as numerical simulation.

2. FBTS METHOD

Maxwell's equations in a nondispersive medium are expressed as

$$L\mathbf{v} = \mathbf{j}, \tag{1}$$

where $\mathbf{v} = (E_x\, E_y\, E_z\, \eta H_x\, \eta H_y\, \eta H_z)^{\mathrm{T}}$, $\mathbf{j} = (\eta J_x\, \eta J_y\, \eta J_z\, 0\, 0\, 0)^{\mathrm{T}}$, $\eta(= \sqrt{\mu_0/\varepsilon_0})$ is the impedance of free space, and the superscript T means transpose. The differential operator L is given by

$$L \equiv \bar{A}\frac{\partial}{\partial x} + \bar{B}\frac{\partial}{\partial y} + \bar{C}\frac{\partial}{\partial z} - \bar{F}\frac{\partial}{\partial (ct)} - \bar{G}, \tag{2}$$

$\bar{F}$ and $\bar{G}$ are constitutive matrixes consisting of relative permittivity ε_r, relative permeability μ_r, and conductivity σ, $\bar{A}$, $\bar{B}$, $\bar{C}$ are 6×6 matrixes consisting of -1, 0, and 1, $c = 1/\sqrt{\varepsilon_0\mu_0}$ is the velocity of light in vacuum.

Consider an inhomogeneous object in homogeneous background. Transmitters in the z-direction at $\mathbf{r}_m^t (m = 1, 2, \ldots, M)$ illuminate the object by a current pulse $J(t)$

$$\mathbf{j}_m = \mathbf{I}_z J(t)\delta(\mathbf{r} - \mathbf{r}_m^t), \tag{3}$$

where $\mathbf{I}_z$ is a unit vector in the z-direction. For each illumination the z-component of time-domain electric field data is collected by receiving antennas in the z-direction at $\mathbf{r}_n^r (n = 1, 2, \ldots, N)$. The distributions of the electrical parameters $\mathbf{p} = (\varepsilon_r\, \mu_r\, \eta\sigma)^{\mathrm{T}}$ are reconstructed from the received data by minimizing the function

$$F(\mathbf{p}) = \int_0^{cT} \sum_{m=1}^{M}\sum_{n=1}^{N} K_{mn}(t)\left|v_m^z(\mathbf{p};\ \mathbf{r}_n^r,\ t) - \tilde{v}_m^z(\mathbf{r}_n^r,\ t)\right|^2 d(ct), \tag{4}$$

where $\tilde{v}_m^z(\mathbf{r}_n^r, t)$ is the observed z-component of electric field at $\mathbf{r}_n^r$ exited by the source $\mathbf{j}_m$, $v_m^z(\mathbf{p}; \mathbf{r}_n^r, t)$ is the calculated z-component of electric field for a guessed parameter $\mathbf{p}$; $K_{mn}(t)$ is a non-negative

weighting function with value of 0 at $t = T$ (T is the duration of observed data).

By introducing an adjoint operator $L^* = -\bar{A}\frac{\partial}{\partial x} - \bar{B}\frac{\partial}{\partial y} - \bar{C}\frac{\partial}{\partial z} + \bar{F}\frac{\partial}{\partial(ct)} - \bar{G}$ of L and an adjoint field $\mathbf{w}_{mn}(\mathbf{p};\ \mathbf{r},\ t)$, the gradients of $F(\mathbf{p})$ to $\mathbf{p}$ are expressed as

$$g_\varepsilon = 2\int_0^{cT} \sum_{m=1}^{M}\sum_{i=1}^{3} w_m^i(\mathbf{p};\mathbf{r},\ t)\ \frac{\partial v_m^i(\mathbf{p};\mathbf{r},\ t)}{\partial(ct)}\ d(ct), \tag{5}$$

$$g_\mu = 2\int_0^{cT} \sum_{m=1}^{M}\sum_{i=4}^{6} w_m^i(\mathbf{p};\mathbf{r},\ t)\ \frac{\partial v_m^i(\mathbf{p};\mathbf{r},\ t)}{\partial(ct)}\ d(ct), \tag{6}$$

$$g_{\eta\sigma} = 2\int_0^{cT} \sum_{m=1}^{M}\sum_{i=1}^{3} w_m^i(\mathbf{p};\mathbf{r},\ t)\ v_m^i(\mathbf{p};\mathbf{r},\ t)\ d(ct), \tag{7}$$

where $w_m^i(\mathbf{p};\ \mathbf{r},\ t) = \sum_{n=1}^{N} w_{mn}^i(\mathbf{p};\ \mathbf{r},\ t)$, and $\mathbf{w}_{mn}(\mathbf{p};\ \mathbf{r},\ t)$ satisfies

$$L^*\mathbf{w}_{mn} = \mathbf{I}_z u_m(\mathbf{p};\ \mathbf{r}_n^r,\ t)\delta(\mathbf{r} - \mathbf{r}_n^r), \tag{8}$$

$$\mathbf{w}_{mn}(\mathbf{p};\ \mathbf{r},\ T) = \mathbf{0}, \tag{9}$$

where $u_m(\mathbf{p};\ \mathbf{r}_n^r,\ t) = K_{mn}(t)[v_m^z(\mathbf{p};\ \mathbf{r}_n^r,\ t) - \tilde{v}_m^z(\mathbf{r}_n^r,\ t)]$ is the weighted residual.

3. NUMERICAL EXAMPLES

3.1. Reconstruction from Synthetic Data

Since the "air phantom" in the next example is lossless, loss is not considered in this example. It does not mean that our reconstruction algorithm is not able to deal with the reconstruction of permittivity and conductivity simultaneously. As shown in Figure 1, in a cylindrical plastic tank oil of relative permittivity 9 is filled; the relative permittivity of the tank is set to $\varepsilon_r = 2.7$. Its outer diameter is 40 cm; height is 40 cm; and thickness of the wall is 1.3 cm. In the oil there are three measurement circles of a diameter of 17.5 cm. Eight 2.7-cm long dipole antennas are set vertically on one of the circles. When one dipole acts as a transmitter, other 7 dipoles are receivers. There are 8 transmitting positions on each measurement circle. The vertical gap of the circle is 2.5 cm. Three sets of data at three different vertical measurement planes are collected with the circular 8-element array. This forms a set of "circular-sliced" data. The total number of transmitter positions is 8×3, and each transmitter has 7 receivers.

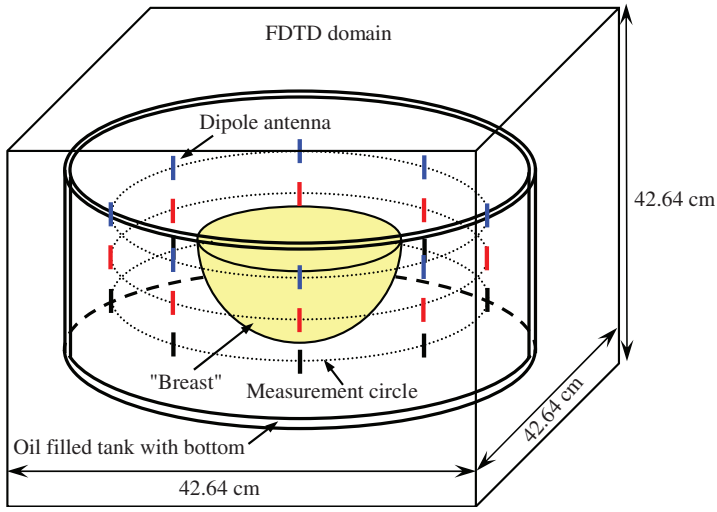

Figure 1. The setup of FDTD simulation.

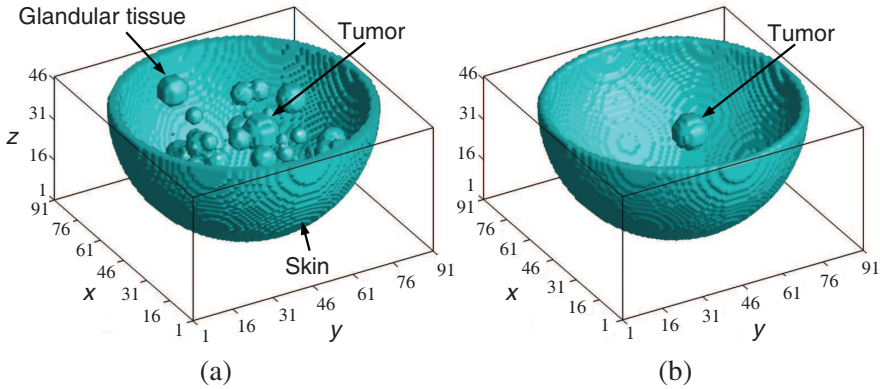

Figure 2. Iso-value surface plot of a breast with a tumor and randomly distributed glandular tissues of random size and permittivity value. The iso-value is (a) $\varepsilon_r = 10$ and (b) $\varepsilon_r = 20$. The coordinates are in grid, the grid size is 1.3 mm.

A hemisphere "breast" is immersed in oil. Figures 2 and 3 show the breast model. Figure 2 is an iso-value surface plot; the iso-value of Figure 2(a) is $\varepsilon_r = 10$; and that of Figure 2(b) is $\varepsilon_r = 20$. Figure 3 is the slice plot; the slices are vertical to the z-axis. The diameter of the "breast" is 11.35 cm including 3.25 mm thick "skin". The relative permittivity of the "skin" is 36, and that of the "normal tissue" is $\varepsilon_r = 9$. Inside the "breast" there are 50 randomly distributed spherical "glandular tissues" with random size ranging between 2.6 mm and 13 mm in diameter and random relative permittivity ranging from $\varepsilon_r = 11$ to $\varepsilon_r = 15$. There is a "tumor" of 1.5 cm in diameter and with relative permittivity of $\varepsilon_r = 50$. The relative permittivity of the "tissues" is listed in Table 1. The index of the axes of Figures 2–4 is a FDTD grid point number.

The "observed" data are calculated by using the FDTD method

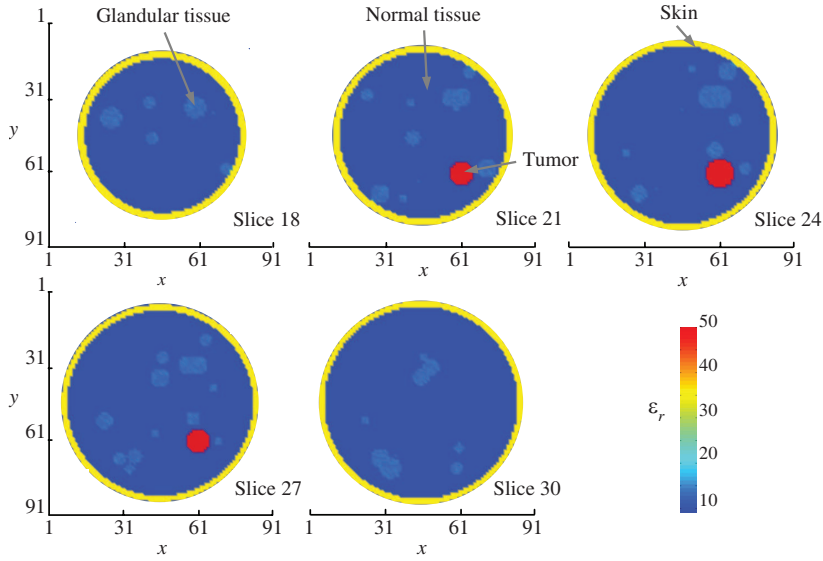

Figure 3. Actual relative permittivity of "breast" slices vertical to the z-axis.

Table 1. Relative permittivity of the numerical examples.

Example	Skin	Glandular tissue	Normal tissue	Tumor	Background
Numerical	36	11–15	9	50	9
Experimental	2.7 (PVC)		1 (styrofoam)	5 (glass)	1 (air)

for the setup shown in Figure 1 and the breast model shown in Figure 2. In the FDTD calculation the grid size is 1.3 mm.

In the reconstruction the tank is not considered. Thus, the background medium is only the oil. The reconstruction region is just the breast. The initial guess of the breast consists of normal tissue and the skin whose position, relative permittivity, and thickness are supposed known. However, during the reconstruction the relative permittivity of the skin is allowed to vary between $\varepsilon_r = 35$ and $\varepsilon_r = 37$.

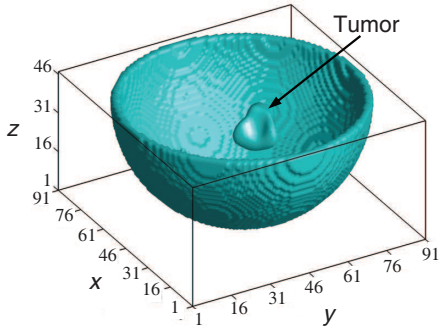

Figure 4. Reconstructed "breast" after 210 iterations from SNR = 20 dB data.

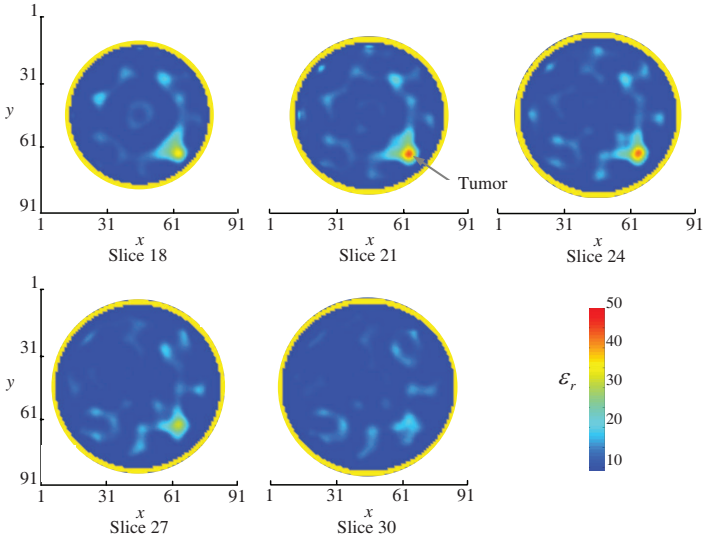

Figure 5. Reconstructed relative permittivity of the "breast" slices after 210 iterations from SNR = 20 dB data.

Figure 4 is the reconstructed iso-value surface plot after 210 iterations, and Figure 5 shows the slices. The iso-value is $\varepsilon_r = 20$. The data are noisy; the signal to noise ratio (SNR) is 20 dB. Figures 4 and 5 show that the tumor is clearly reconstructed. The position is correct; however the shape is little bit deformed. The maximum value of relative permittivity is larger than 45.

Each iteration of the synthetic example took about 114 minutes using 4-CPU MPI parallel calculation on Fujitsu Primequest 580 (Intel Itanium2 1.6 GHz Processor). The FDTD domain is a 153-grid cube; the reconstruction region is $91 \times 91 \times 47$ grids; and the number of time steps is 1800.

3.2. Reconstruction from Experimental Data

An "air phantom" is constructed from a section of PVC pipe, styrofoam, and glass as the object to be imaged. The phantom is designed to have a geometry and relative permittivity relationships among the materials that resembled those in the breast as follows: PVC pipe ($\varepsilon_r \approx 2.7$) to stand for skin ($\varepsilon_r \approx 40.0$), styrofoam ($\varepsilon_r \approx 1.0$) to stand for fat ($\varepsilon_r \approx 10$), and glass ($\varepsilon_r \approx 5.0$) to stand for tumors ($\varepsilon_r \approx 50$). The dielectric constants are listed in Table 1 too. A glass cylinder with a height of 5 cm and a diameter of 0.96 cm is inserted into the styrofoam in the z-axis to represent a tumor, and the FBTS technique is utilized to determine whether the phantom could be reconstructed and the tumor detected from measured electric field. The loss of all materials is assumed to be negligible.

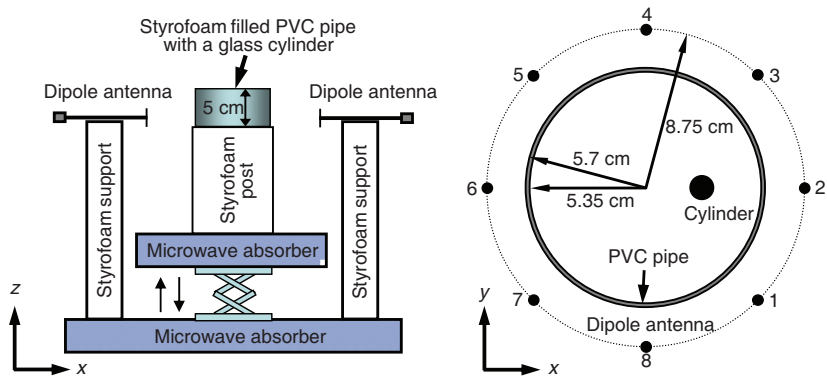

Figure 6. Measurement setup for characterization of air phantom: (a) diagram of side view, (b) diagram of top view.

The configuration of transmitters and receivers are the same as that shown in Figure 1. The phantom is aligned on top of a vertically adjustable platform in the center of the antenna array, as shown in Figure 6. The wire dipole antennas are constructed from semi-rigid coaxial cable of 0.086 inch in diameter. A Z5623A 8-channel Multi-port Test Set (Agilent Technologies, Palo Alto, CA, USA) and an E8358 Performance Network Analyzer (Agilent Technologies) are connected to the antennas to allow multi-path scattering parameter measurements. Software is written in LabView (National Instruments, Dallas, TX, USA) to control the switching and data collection process, resulting in a fully automatic scattering measurement system.

The object is characterized at vertical planes near the top, middle, and bottom of the pipe. The measured scattering data in the frequency domain are transformed into the time domain, and the transformed data are utilized by the 3-D FBTS algorithm to reconstruct an image of the air phantom. The bandwidth of the received signal is 2.99–6.97 GHz at which its amplitude is 5% of the maximum amplitude at 4.67 GHz. It is assumed that the location and approximate permittivity value of the "skin" can be estimated before reconstruction by other means. To reduce reconstruction time, the top and bottom scattering measurements were assumed to be equivalent for the reconstruction (i.e., a symmetry plane normal to the xy-plane is utilized). A 1.3 mm×1.3 mm×1.3 mm FDTD grid was utilized and the imaging algorithm is run for 22 iterations.

Results for the reconstruction based on the scattering measurements of the air-phantom are shown in Figures 7 and 8 where the sections pass through the phantom's center. These figures show successful reconstruction of the cylinder appearing at the center of the pipe (Figure 7) and at the middle of its radius (Figure 8), respectively. The reconstructed peak permittivity is $\varepsilon_r = 5.36$ in Figure 7, and $\varepsilon_r = 5.35$ in Figure 8. The horizontal cross-sectional shape of the cylinder (Figures 7(a) and 8(a)) is a well-formed circle, and the vertical cross-section of the reconstructed cylinder also matches the actual shape very well as shown in Figures 7(b) and 8(b).

The estimated center position of the cylinder is the center of the high reconstructed permittivity values, and the actual position is shown as a white cross. The estimates match the actual measured position in the phantom quite well. In Figure 8, several clutter signals exist. The reconstructed images in Figures 7 and 8 are slightly longer in the z-direction than the actual one because of the observation geometry. The cylinder is slightly deformed in Figure 8(a).

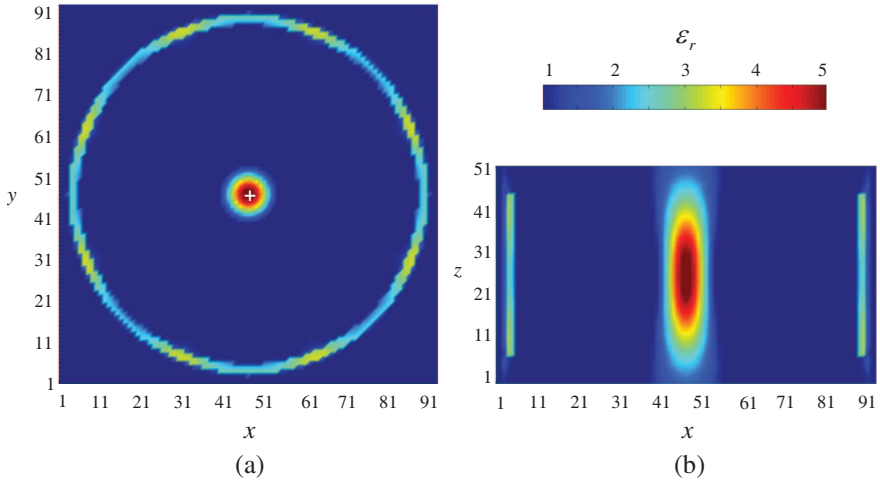

Figure 7. Reconstructed relative permittivity of the air phantom with a glass cylinder at the center: (a) xy-plane, (b) xz-plane. The cross represents its measured position.

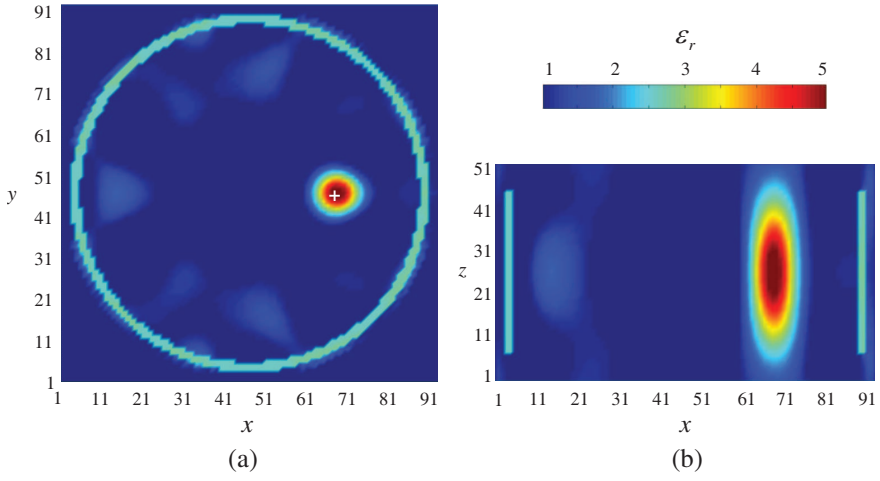

Figure 8. Reconstructed relative permittivity of the air phantom with a glass cylinder offset to the center: (a) xy-plane, (b) xz-plane. The cross represents its measured position.

4. DISCUSSION

We use the "circular-sliced" configuration of three measurement circles. This vertically scanned circular antenna array configuration is advantageous for practical implementation [5, 9]. However, a potential shortcoming of this approach is the fact that no "cross-plane" measurements are possible, resulting in less precise vertical resolution of a tumor [26]. It is seen from Figures 7(b) and 8(b) that the "tumor" is with a slightly stretched shape along the z-axis.

In our reconstruction examples, we suppose that the position of the breast and thickness can be detected before the reconstruction by other means. This assumption greatly reduces iteration time and improves solution quality. In a matter of fact, some microwave technologies are under development to estimate the thickness of skin [27], the average breast tissue properties [28], and breast location [29].

Our future challenges for the FBTS technique are speeding up the algorithm and developing FBTS algorithm for dispersive cases.

5. CONCLUSION

From the reconstruction examples using synthetic and experimental data it is seen that the quantitative detection of breast cancer is possible by using the FBTS method. For the synthetic reconstruction example the oil is used in order to increase the energy penetrating the breast. In order to simplify the reconstruction, the influence of the tank has not been taken into account. That the breast is successfully reconstructed and the tumor is detected indicates that 40 cm tank is large enough for practical experiment.

ACKNOWLEDGMENT

This work was supported in part by the National Natural Science Foundation of China under Grant-in-Aid 40574053, the Program for New Century Excellent Talents in University, China (NCET-06-0602), and the State Key Laboratory of Petroleum Resources and Prospecting, China.

REFERENCES

1. Davis, S. K., B. D. Van Veen, S. C. Hagness, and F. Kelcz, "Breast tumor characterization based on ultrawideband microwave backscatter," *IEEE Transactions on Biomedical Engineering*, Vol. 55, No. 1, 237–246, 2008.

2. Guo, B., Y. Wang, J. Li, and P. Stoica, "Microwave imaging via adaptive beamforming methods for breast cancer detection," *Journal of Electromagnetic Waves and Applications*, Vol. 20, No. 1, 53–63, 2006.
3. Takenaka, T., H. Zhou, and T. Tanaka, "Inverse scattering for a three-dimensional object in the time domain," *J. Opt. Soc. Am. A*, Vol. 20, No. 10, 1867–1874, 2003.
4. Fear, E., J. Sill, and M. Stuchly, "Experimental feasibility study of confocal microwave imaging for breast tumor detection," *IEEE Trans. Microw. Theory Tech.*, Vol. 51, No. 3, 887–892, 2003.
5. Li, D., P. Meaney, T. Raynolds, S. Pendergrass, M. Fanning, and K. Paulsen, "Parallel-detection microwave spectroscopy system for breast imaging," *Review of Scientific Instruments*, Vol. 75, No. 7, 2305–2313, 2004.
6. Zhang, H., S. Y. Tan, and H. S. Tan, "A novel method for microwave breast cancer detection," *Progress In Electromagnetics Research*, PIER 83, 413–434, 2008.
7. Zainud-Deen, S. H., W. M. Hassen, E. M. Ali, K. H. Awadalla, and H. A. Sharshar, "Breast cancer detection using a hybrid finite difference frequency domain and particle swarm optimization techniques," *Progress In Electromagnetics Research B*, Vol. 3, 35–46, 2008.
8. Fang, Q., P. Meaney, S. Geimer, A. Streltsov, and K. Paulsen, "Microwave image reconstruction from 3-D fields coupled to 2-D parameter estimation," *IEEE Trans. Med. Imag.*, Vol. 23, No. 4, 475–484, 2004.
9. Meaney, P., M. Fanning, T. Raynolds, C. Fox, Q. Fang, et al., "Initial clinical experience with microwave breast imaging in women with normal mammography," *Academic Radiology*, Vol. 14, No. 2, 207–218, 2007.
10. Poplack, S., T. Tosteson, W. Wells, B. Pogue, P. Meaney, et al., "Electromagnetic breast imaging: Results of a pilot study in women with abnormal mammograms," *Radiology*, Vol. 243, No. 2, 350–359, 2007.
11. Sill, J. and E. Fear, "Tissue sensing adaptive radar for breast cancer detection — Experimental investigation of simple tumor models," *IEEE Trans. Microw. Theory Tech.*, Vol. 53, No. 11, 3312–3319, 2005.
12. Bond, E., X. Li, S. Hagness, and B. Van Veen, "Microwave imaging via space-time beamforming for early detection of breast cancer," *IEEE Trans. Antennas and Propagat.*, Vol. 51, No. 8, 1690–1705.

13. Li, X., S. Davis, S. Hagness, D. D. Van Weide, and B. Van Veen, "Microwave imaging via space-time beamforming: Experimental investigation of tumor detection in multilayer breast phantoms," *IEEE Trans. Microw. Theory Tech.*, Vol. 52, No. 8, 1856–1865, 2004.
14. Hagness, S. C., A. Taflove, and J. E. Bridges, "Two-dimensional FDTD analysis of a pulsed microwave confocal system for breast cancer detection: Fixed-focus and antenna-array sensors," *IEEE Transactions on Biomedical Engineering*, Vol. 45, 1470–1479, 1998.
15. Hagness, S. C., A. Taflove, and J. E. Bridges, "Three-dimensional FDTD analysis of a pulsed microwave confocal system for breast cancer detection: Design of an antenna-array element," *IEEE Trans. Antennas and Propagat.*, Vol. 47, 783–791, 1999.
16. Lazebnik, M., D. Popovic, L. McCartney, C. B. Watkins, M. J. Lindstrom, et al., "A large-scale study of the ultrawideband microwave dielectric properties of normal, benign and malignant breast tissues obtained from cancer surgeries," *Phys. Med. Biol.*, Vol. 52, 6093–6115, 2007.
17. Lazebnik, M., L. McCartney, D. Popovic, C. M. J. Lindstrom, et al., "A large-scale study of the ultrawideband microwave dielectric properties of normal breast tissue obtained from reduction surgeries," *Phys. Med. Biol.*, Vol. 52, 2637–2656, 2007.
18. Zastrow, E., S. K. Davis, M. Lazebnik, F. Kelcz, B. D. Van Veen, and S. C. Hagness, "Development of anatomically realistic numerical breast phantoms with accurate dielectric properties for modeling microwave interactions with the human breast," *IEEE Transactions on Biomedical Engineering*, Vol. 55, No. 12, 2792–2800, 2008.
19. Van Dongen Koen, W. A. and W. M. D. Wright, "A full vectorial contrast source inversion scheme for three-dimensional acoustic imaging of both compressibility and density profiles," *The Journal of the Acoustical Society of America*, Vol. 121, 1538–1549, 2007.
20. Caorsi, S., G. L. Gragnani, and M. Pastorino, "Redundant electromagnetic data for microwave imaging of three-dimensional dielectric objects," *IEEE Trans. Antennas and Propagat.*, Vol. 42, No. 5, 581–589, 1994.
21. Lin, J.-H. and W. C. Chew, "Solution of the three-dimensional electromagnetic inverse problem by the local shape function and the conjugate gradient fast Fourier transform methods," *J. Opt. Soc. Am. A*, Vol. 14, No. 11, 3037–3045, 1997.
22. Semenov, S. Y., R. H. Svenson, A. E. Bulyshev, et al., "Three-

dimensional microwave tomography: Experimental prototype of the system and vector Born reconstruction method," *IEEE Transactions on Biomedical Engineering*, Vol. 46, No. 8, 937–946, 1999.

23. Abubakar, A., P. M. D. Van Berg, and B. Kooij, "A conjugate gradient contrast source technique for 3D profile inversion," *IEICE Trans. Electron.*, Vol. E83-C, 1864–1874, 2000.
24. Yee, K. S., "Numerical solution of initial boundary value problems involving Maxwell's equations in isotropic media," *IEEE Trans. Antennas and Propagat.*, Vol. 14, 302–307, 1966.
25. Taflove, A. and S. C. Hagness, *Computational Electrodynamics: The Finite-difference Time-domain Method*, 3rd edition, Artech House, Norwood, MA, 2005.
26. Meaney, P., Q. Fang, and K. Paulsen, "Data collection strategies and their impact on 3-D microwave imaging of the breast," *IEEE Antennas and Propagation Society International Symposium*, Vol. 1B, 183–186, 2005.
27. Winters, D. W., E. J. Bond, B. D. Van Veen, and S. C. Hagness, "Estimation of the frequency-dependent average dielectric properties of breast tissue using a time-domain inverse scattering technique," *IEEE Trans. Antennas and Propagat.*, Vol. 54, No. 11, 3517–3528, 2006.
28. Williams, T., E. Fear, and D. Westwick, "Tissue sensing adaptive radar for breast cancer detection- investigations of an improved skin-sensing method," *IEEE Trans. Microw. Theory Tech.*, Vol. 54, No. 4, 1308–1314, 2006.
29. Winters, D., J. Shea, E. Madsen, G. Frank, B. Van Veen, and S. Hagness, "Estimation of the frequency-dependent average dielectric properties of breast tissue using a time-domain inverse scattering technique," *IEEE Transactions on Biomedical Engineering*, Vol. 55, No. 1, 247–256, 2008.